Predicted and Projected Water Resources Changes in the Chari Catchment, the Lake Chad Basin, Africa

RASHID MAHMOOD

Key Laboratory of Water Cycle and Related Land Surface Processes, Institute of Geographic Science and Natural Resources Research, Chinese Academy of Sciences, Beijing, China

SHAOFENG JIA

Key Laboratory of Water Cycle and Related Land Surface Processes, Institute of Geographic Science and Natural Resources Research, Chinese Academy of Sciences, Beijing, and Qinghai Key Laboratory of Basin Water Cycle and Ecology, Qinghai Institute of Water Resources and Hydropower, and School of Geographical Sciences, Qinghai Normal University, Xining, China

TARIQ MAHMOOD

State Key Laboratory of Numerical Modelling for Atmospheric Sciences and Geophysical Fluid Dynamics, Institute of Atmospheric Physics, Chinese Academy of Sciences, and University of Chinese Academy of Sciences, Beijing, China, and Pakistan Meteorological Department, Islamabad, Pakistan

ASIF MEHMOOD

Key Laboratory of Water Cycle and Related Land Surface Processes, Institute of Geographic Science and Natural Resources Research, Chinese Academy of Sciences, and University of Chinese Academy of Sciences, Beijing, China

(Manuscript received 16 May 2019, in final form 12 October 2019)

ABSTRACT

The water resources of the Chari River basin, contributing more than 90% of the water to one of the largest lakes in Africa, known as Lake Chad, are highly vulnerable to natural and anthropogenic changes. Therefore, the changes in water resources were predicted for the next 20 years (i.e., 2016–35) by using the harmonic regression model (HRM), one of the most sophisticated time series methods, and also projected under representative concentration pathways (RCPs) by using the multimodel approach for the periods 2021–50, 2051–80, and 2081–2100, with respect to the baseline period (1971–2001). The Tropical Rainfall Measuring Mission (TRMM), Climatic Research Unit (CRU), and dynamically downscaled climatic data were used in the analysis of the present study. The results showed that under MME-RCP2.6 (multimodel ensemble of RCMs), low flow (average of low-flow months, December–July), high flow (August–November), and annual flow were projected to decrease in the future. In contrast, under MME-RCP4.5 and MME-RCP8.5, high and annual flows were projected to increase in all three time horizons, while low flow will decrease except in 2021–50 under MME-RCP8.5. In the next two decades, the HRM showed decrease in all type of flows (low, high, and annual), very similar to the results under MME-RCP2.6 for the same period. In contrast, almost all flows are expected to increase under MME-RCP4.5 and MME-RCP8.5 in the next two decades. On the whole, the flows are expected to decrease under the HRM and RCP2.6 but to increase under RCP4.5 and RCP8.5.

1. Introduction

Lake Chad, one of the largest lakes in Africa, is an important freshwater source for pastoral land, agriculture, and fishing, and it is located in the center of the world's largest endorheic basin (a drainage basin that does not flow to other external water bodies such as

rivers or oceans), the Lake Chad basin (LCB) (Buma et al. 2016). The water resources of the LCB provide livelihoods to more than 45 million people (Komble et al. 2016), which are mostly consumed by agriculture. Approximately 60% of the population is reliant on agricultural sector (UNEP 2006). However, the water resources of the basin are exceptionally vulnerable to the impact of environmental changes (Rizzo 2015). For example, in the 1960s, LC was the world's sixth largest inland water body with a water surface area of $25\,000\,km^2$, and since then, it has shrunk to a water surface area of $2000\,km^2$ (water covered by aquatic vegetation is not included) during the last 40 years (Coe and Foley 2001; LCBC 2011; Leblanc et al. 2011). Moreover, its water surface reduced to $300\,km^2$ in the 1980s (Gao et al. 2011). Furthermore, the lake not only shrunk, it split into the northern (small) and southern (big) lakes in 1975. The main reason for the lake splitting is reported as the consequence of an overwhelming drought that occurred over the Sahel belt in the 1970s (Lemoalle et al. 2012). Lake Chad's vulnerability is mainly attributed to decreasing discharge of the Chari River because more than 90% water to the lake comes from it (Gao et al. 2011; Lemoalle and Magrin 2014). According to Coe and Foley (2001), the discharge of the Chari River has decreased by approximately 75% from 1960 to 2001. On the other hand, Mahmood and Jia (2019) showed approximately 57% decrease in discharge at N'Djamena during 1951–2013 because an increasing trend in rainfall has been observed after 1990. The decreasing discharge of the Chari River is mainly attributed to changing climate and anthropogenic activities (Coe and Foley 2001; Mahmood and Jia 2019). So rapidly changing climate can definitely change the discharge of the river, and consequently, can have large impacts on the water resources of Lake Chad. Therefore, a comprehensive study is essential to predict the discharge of the Chari River for short-term planning and to project the discharge under different emission scenarios for long-term planning in the basin.

For the assessment of projected changes in water resources, the outputs from the state-of-the-art global climate models (GCMs) are being used throughout the world (Ahmadalipour et al. 2017; Mahmood and Jia 2016). However, their outputs are coarse in spatial resolution (e.g., 100–300 km) (Zubler et al. 2016), which limits the application of these models in environmental and hydrological assessment studies on a basin scale (Gädeke et al. 2014; Mahmood et al. 2018). Nonetheless, these problems can be minimized by using regional climate models (RCMs), which downscale the outputs of GCMs to a finer scale (5–50 km) and provide required information on a basin level needed for impact

assessment studies (Diallo et al. 2012). However, another key problem is that the outputs of both RCMs and GCMs suffer from the existence of considerable uncertainties from differences sources, such as projected GHG emission for future, model parameterization, and internal dynamics as well as physics, natural internal climate variability, and so on (Giorgi 2005; Haensler et al. 2013; Tebaldi and Knutti 2007). To minimize the effect of these kinds of uncertainties, an ensemble of climate projections from a range of climate models, as contrasting to a single scenario of a single model, is considered necessary for the projection of climate and impacts assessment studies (Tebaldi and Knutti 2007). This approach is referred to as a multimodel approach. By using this approach, researchers expect to accomplish two related objectives. First, they want simulation agreement across models in the ensemble to imply robustness, for any particular phenomenon of interest or, more generally, to gain an understanding of the structural uncertainty in any prediction. Second, and more ambitiously, they would like the distribution of the behavior of any particular phenomenon across the ensemble to be a reasonable approximation of the probability of its occurrence, conditional upon the assumptions described above (Abramowitz et al. 2019). This approach is well accepted within the scientific community to achieve robust climate information for a specific region (Haensler et al. 2013). Many studies, such as Diallo et al. (2012), Endris et al. (2016), Haensler et al. (2013), Landman and Beraki (2012) Losada et al. (2010), Nikiema et al. (2017), Aich et al. (2014), Bodian et al. (2018), Karambiri et al. (2011), and Mahé et al. (2008), have reported this approach for the projection of climate and to assess the anticipated discharge changes in different regions of Africa. However, we could not find some well-documented studies in the literature on the assessment of projected streamflow changes in the main river, the Chari River, of Lake Chad under different representative concentration pathways (RCPs), using a multimodel approach.

Although the projected water resources are important for longer-period (50–100 years) water resources planning, the prediction of water resources in the near future (10–20 years) is even more essential for policy-makers and planners to minimize the impacts of climate change on water resources by adopting some proper mitigative and adaptive actions. Additionally, the prediction can also help to resolve many other issues related to floods and droughts, water availability, water supply and demand, reservoir maintenance, natural disasters, etc. (Feng et al. 2016; Nury et al. 2013; Sunday et al. 2014; Reyna et al. 2015). For short-term prediction and forecasting, a time series modeling (time series analysis)

is one of the major tools (Nury et al. 2013; Soltani et al. 2007) that is applied in different research fields such as weather and hydrological forecasting, the prediction of market potential, controlling environmental pollution, and oceanography (Prins 2012; Yang and Lu 2011). Different time series methods have been reported in the literature for forecasting and predicting the near-future events. Some are very simple such as autoregressive model, moving average model, combination of moving average and autoregressive, exponential smoothing, and seasonal decomposition, and some are very complex and sophisticated, such as neural network and spectral analysis (Hill et al. 2006). Some time series, such as rainfall, are mostly chaotic because these are composed of different components, for example, period patterns, trends, cyclic behavior, and white noise, which limits the application of simple time series methods. The prediction of such kinds of variables is mainly accomplished with some sophisticated techniques such as spectral analysis and neural network (Grzesica and Więcek 2016).

It is clear from the above discussion that both prediction and projection are equally important for the better water resources management and planning for a basin like the Chari River basin, where the water resources are under great threats of changing climate. Therefore, in the present study, the changes in the water resources of the Chari River basin, the main feeder of Lake Chad, were predicted for short term planning and projected for long term planning in the basin. The projected changes were assessed under three emission scenarios (i.e., RCP2.6, RCP 4.5, and RCP 8.5) by using multimodel approach for three time horizons (i.e., 2021–50, 2051–80, and 2081–2100) with respect to the baseline period (1971–2000); and the predicted changes were assessed for the next two decades (i.e., 2016–25 and 2026–35) relative to the baseline period by using a sophisticated time series technique known as the spectral analysis. Since the observed climate data are so sparse and not of high quality, the Tropical Rainfall Measuring Mission (TRMM) and the Climatic Research Unit (CRU) datasets were used in calibration and validation of hydrological model and in spectral analysis, respectively. Dynamically downscaled climatic data was obtained from Coordinated Regional Climate Downscaling Experiment (CORDEX) for the twenty-first century and used in the projection analysis.

2. Study area and data

a. Study area

The Chari River basin (CRB) is a transboundary river basin located in the largest endorheic basin, the LCB.

The CRB straddles the boarders of Chad, Sudan, Central African Republic, and Cameroon (as shown in Fig. 1) and covers an area of $690\,000\,km^2$, which is approximately 27% of the LCB's area ($2.5 \times 10^6\,km^2$) (Coe and Foley 2001; Gao et al. 2011; Mahmood and Jia 2019; Komble et al. 2016). The LCB is divided into four main climatic zones moving from south to north: the Sudano–Guinean (rainfall ranges between 600 and 1500 mm), Sahelo–Sudania (rainfall between 400 and 600 mm), Sahelo–Saharan (rainfall between 100 and 400 mm), and Saharan (rainfall less than 100 mm) zones. Among them, the CRB is located in the first two zones, which receive rainfall between 400 mm (the northern parts of the CRB) and 1500 mm (the southern parts of the CRB) (Komble et al. 2016). The Chari River moves into the southern pool of Lake Chad near N'Djamena, as shown in Fig. 1, where it drains all of its water to Lake Chad, with an average annual flow of $27.14\,km^3$ (Lemoalle et al. 2012). The Chari River contributes more than 90% of the total inflow of the lake, and the rest of the inflow of the lake comes from the Komadugu, Ngadda, Yobe, Yedseram, El-Beid, and Gubio Rivers (Gao et al. 2011; Lemoalle and Magrin 2014; Komble et al. 2016).

b. Hydrometeorological data

Monthly discharge data of the N'Djamena (1951–2013), Sarh (2001–07), and Bongor (2001–07) hydrometric stations was gathered from the Lake Chad Basin Commission (locations of these stations shown in Fig. 1). Since measured climatic data are sparse and of low quality in the basin, daily rainfall for the period of 2001–15 (for hydrological modeling) and monthly climatic data (i.e., rainfall, maximum and minimum temperatures, and wet days) for 1951–2015 (for time series analysis) were attained from TRMM_3B42RT_daily_V7 (https://mirador.gsfc.nasa.gov) and CRU-TS4.00 (Harris et al. 2014) datasets, respectively. The CRU data have a spatial resolution of 0.5° × 0.5°, with a monthly time step. It includes all necessary climate variables such as rainfall, temperature, and potential evapotranspiration. Many studies have used this dataset for climatic analysis and the verification of GCMs, RCMs, and hydrological models' simulations in the regions where station-based observations are lacked (Miao et al. 2014; McMahon et al. 2015; Smiatek et al. 2009). On the other hand, TRMM is a joint product of U.S. National Aeronautics and Space Administration (NASA) and the Japan Aerospace Exploration Agency (JAXA), which covers a land area of 50°S–50°N and has spatial resolution of 0.25° × 0.25°. Since TRMM carries a rainfall radar (PR) along with the TRMM Microwave Imager (TMI) and Visible and Infrared
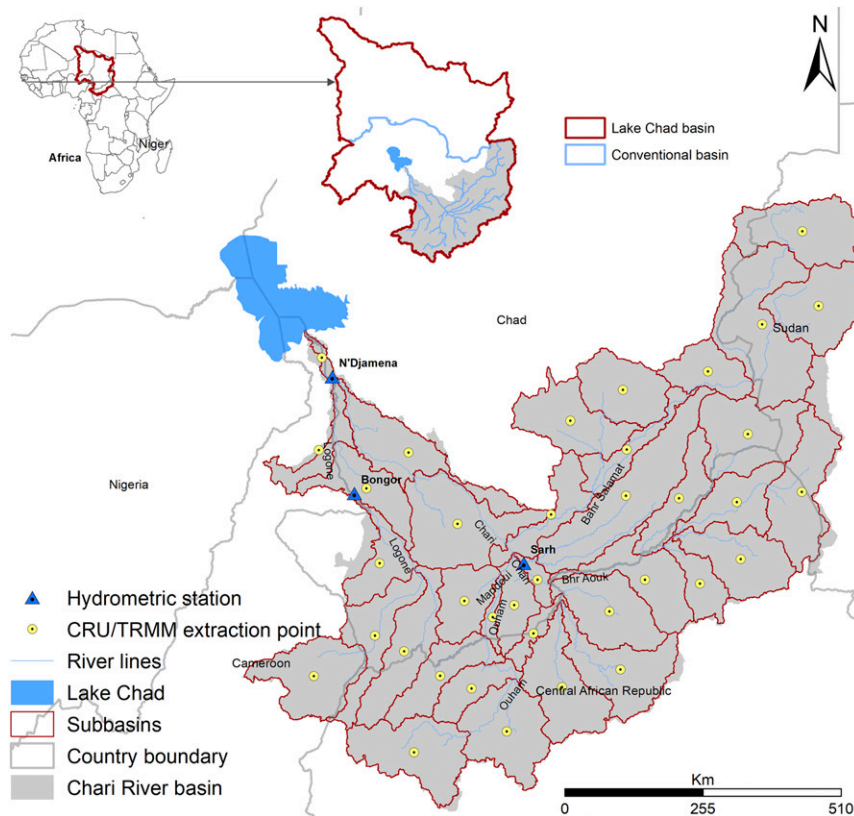
FIG. 1. Location map of the Chari River basin, showing the extracted CRU/TRMM climate data points, observed hydrometric station, and subbasins.

Scanner (VIRS) and can provide three-dimensional rainfall distribution in an unprecedented way, it may provide more accurate rainfall estimates than previous space-borne sensors. Therefore, TRMM rainfall is acknowledged as more reliable data than obtained from other satellites (Gu et al. 2010) and has been increasingly using in hydrological modeling during the last few years, as in Collischonn et al. (2008), Gu et al. (2010), He et al. (2017), Hughes (2006), Liu et al. (2017), Meng et al. (2014), and Zhu et al. (2018), especially in the sparsely gauged basins, with no appropriate temporal and spatial resolution for hydrological modeling. So satellite-based rainfall has provided hydrologists a potential alternative for hydrological applications since the last few years (Zhu et al. 2018). The CRU and TRMM extraction points are shown in Fig. 1.

c. Land cover, soil, and elevation data

Land cover can have a great effect on hydrologic processes of a basin, especially the density of plant cover and the morphology of plant species can greatly influence these processes (Ghoraba 2015). The land cover/land use data (Global Land Cover Characterization) and soil

data were obtained from U.S. Geological Survey (USGS; https://earthexplorer.usgs.gov) and Harmonized World Soil Database (http://www.fao.org/soils-portal/soil-survey/soil-maps-and-databases/harmonized-world-soil-database-v12/en/), respectively. Other important data required for hydrological modeling are elevation data, which are necessary to extract geomorphological information of a territory. For this purpose, a DEM of NASA's Shuttle Radar Topography Mission (SRTM) was extracted from the USGS (https://earthexplorer.usgs.gov) for the CRB. It covers most parts of the world, with a spatial resolution of 3 arc s.

d. Downscaled GCM climate data

To date, a multimodel ensemble is considered the only option to judge the plausibility of climate model outputs (Schaefli 2015) because there are intermodel differences in internal physics and the process of parameterization of variables (Rajib et al. 2014). Therefore, in the present study, a multimodel and multiscenario approach was adopted for plausible climate projections and to consider uncertainties in projections. So downscaled climate data (i.e., rainfall and temperature) was obtained from CORDEX for the African domain, for all available

GCMs driven by RCMs (Table 1). The downscaled data was obtained for the historical period (1971–2005) and the future period (2005–2100) under RCP2.6, RCP4.5, and RCP8.5. Under RCP2.6, climate forcing (radiative forcing) will reach a peak level (i.e., 3.1 W m^{-2}) by the mid-twenty-first century and then decline to 2.6 W m^{-2} by the end of twenty-first century (van Vuuren et al. 2011). This can be described as limiting anthropogenic climate change by reducing emission of GHGs in the coming few years, which requires a major turnaround in climate policies. RCP4.5 is described as a stabilization scenario because the climate forcing will stabilize before the twenty-first century due to the implementation of a range of strategies and technologies for the reduction of emission of GHGs. However, RCP8.5 describes a continuous increase in GHGs, where radiative forcing will reach to 8.5 W m^{-2} by the twenty-first century and will continue at the same rate (Moss et al. 2010; van Vuuren et al. 2011). RCP6.0 was not included in the present study because it is similar to RCP4.5 except it stabilizes after the twenty-first century.

Eleven datasets were obtained under the RCP2.6 experiment, which were created by downscaling seven GCMs with two RCMs, as described in Table 1. Similarly, 15 and 18 datasets were attained under the RCP4.5 and RCP8.5 experiments, respectively, which were produced by downscaling 11 GCMs with 3 RCMs (Table 1). The historical datasets were obtained in accordance with RCPs (Table 1), which were used for correcting biases in the present study. The CORDEX climate products were created by downscaling the state-of-the-art GCMs (used in CMIP5 project) with different RCMs (Taylor et al. 2012) under the latest generation of emission scenarios known as RCPs (Moss et al. 2010). For the African domain, all downscaled data are provided at 0.44° spatial resolution for the period of 1951–2005 under the historical experiment and for 2006–2100 under RCPs.

3. Methodology

a. Setup of hydrologic model

A hydrological model used in the present study is Hydrologic Engineering Center–Hydrologic Modeling System (HEC-HMS). The U. S. Army Corps of Engineers developed this model (Scharffenberg and Fleming 2010) to deal with different hydrological purposes, for example, flood modeling, natural flow simulation, flood forecasting, and watershed planning and management, and it has been applied throughout the world under different climatic and topographic conditions, such as in Halwatura and Najim (2013), Mahmood and Jia (2017),

Meenu et al. (2012), Ramly and Tahir (2016), Verma et al. (2010), Yimer et al. (2009), and Zema et al. (2017). There are four major components of this model: 1) a basin model, which contains all of the information about a basin's physical features like the basin's area and river lengths; 2) a meteorological model to calculate the spatial distribution of climate variables; 3) a control specification to run the model for different simulation time periods; and 4) a data manager that stores a time series of climatic variables, for example, discharge, wind speed, temperature, and rainfall (Verma et al. 2010; Scharffenberg and Fleming 2010). More detail is provided in the technical reference manual and user's manual of the model (Feldman 2000; Scharffenberg and Fleming 2010).

According to the objectives of the study, the deficit and constant loss method (DCLM), Clark unit hydrograph, constant monthly baseflow method (CMBM), Muskingum routing method (MRM), and Penman–Monteith method (PMM) were included in the model setup, as in Mahmood and Jia (2019), García et al. (2008), Halwatura and Najim (2013), Meenu et al. (2012), and Verma et al. (2010). The DCLM is a single layer continuous method, which calculates the surplus rainfall by removing the losses (e.g., infiltration) from total rainfall. The excess rainfall from the DCLM is converted into direct runoff using the Clark method, which is a synthetic unit hydrograph. In the CMBM, constant baseflow values are used for each month, which remains constant throughout the simulation period, as a major assumption of this method. In the present study, baseflow was calculated for each month using a baseflow separation method developed by Lyne and Hollick (1979). It has been designed as a means of analyzing the time-dependent and slow stream responses to precipitation. The method assumes high-frequency signals to represent direct runoff, while low-frequency signals are associated with the baseflow component (Lyne and Hollick 1979). The Muskingum method, which is a simple form of mass conservation, routes total discharge (baseflow + direct runoff) from one point to the other in the main streams (Scharffenberg and Fleming 2010). The model setup for the CRB includes the following eight parameters, which were optimized using a calibration and validation process to develop the model for the basin: Muskingum time of travel, maximum deficit, initial deficit, storage coefficient, time of concentration, infiltration rate, Muskingum's coefficient, and percentage of imperviousness. Before starting calibration process, the initial values of these parameters, which are required to run the model, were estimated using land use land cover data, soil data, and basin characteristics, as in Ahbari et al. (2018).

TABLE 1. RCM simulations under RCP2.6, RCP4.5, and RCP8.5, obtained from CORDEX for the historical (1971–2000) and future (2006–2100) periods.

Model name	Institution name	Institution acronym	RCM–GCM for RCPs		
			RCP2.6 and historic	RCP4.5 and historic	RCP8.5 and historic
RCM					
CLMcom-CLMcom-8–17	Climate Limited-area Modeling Community (CLM-Community)	CLMcom	GERICS-GFDL	SMHI-CCCma	SMHI-CCCma
GERICS-GERICS	Helmholtz-Zentrum Geesthacht, Climate Service Center Germany	GERICS	SMHI-MOHC	CLMcom-CNRM	CLMcom-CNRM
SMHI-RCA4	Swedish Meteorological and Hydrological Institute, Rossby Centre	SMHI	GERICS-MOHC	SMHI-CNRM	SMHI-CNRM
GCM			SMHI-ICHEC	SMHI-CSIRO	SMHI-GFDL
CanESM2	Canadian Centre for Climate Modeling and Analysis (Canada)	CCCma	GERICS-ICHEC	SMHI-GFDL	CLMcom-ICHEC
CNRM-CM5	Centre National de Recherches Meteorologiques (France)	CNRM	GERICS-IPSL	CLMcom-MOHC	SMHI-ICHEC
CSIRO Mk3.6.0	Commonwealth Scientific and Industrial Research Organization (Australia)	CSIRO	SMHI-MIROC	SMHI-MOHC	GERICS-ICHEC
EC-EARTH	Irish Centre for High-End Computing (Ireland)	ICHEC	GERICS-MIROC	CLMcom-ICHEC	SMHI-IPSL
GFDL-ESM2G	Geophysical Fluid Dynamics Laboratory (United States)	GFDL	SMHI-MPI	SMHI-ICHEC	GERICS-IPSL
HadGEM2-ES	Met Office Hadley Centre (United Kingdom)	MOHC	GERICS-MPI	SMHI-IPSL	SMHI-MIROC
IPSL-CM5A-LR	Institut Pierre Simon Laplace (France)	IPSL	SMHI-NCC	SMHI-MIROC	GERICS-MIROC
IPSL-CM5A-MR	Institut Pierre Simon Laplace (France)	IPSL		CLMcom-MPI	CLMcom-MOHC
MIROC5	Center for Climate System Research, The University of Tokyo, National Institute for Environmental Studies, Japan Agency for Marine-Earth Science and Technology (Japan)	CCSR, NIES, JAMSTEC		SMHI-MPI	SMHI-MOHC
MPI-ESM-LR	Max Planck Institute for Meteorology	MPI-M		GERICS-MPI	GERICS-MOHC
NorESM1-M	Norwegian Climate Centre (Norway)	NCC		SMHI-NCC	CLMcom-MPI
					SMHI-MPI
					GERICS-MPI
					SMHI-NCC

b. Calibration and validation of hydrologic model

The model's calibration was performed for the period 2001–03 at the N'Djamena, Sarh, and Bongor stations, and validation for 2004–13 at N'Djamena and for 2004–07 at Sarh and Bongor, using the TRMM data. Before calibration, it is important to explore the sensitive parameters. For this purpose, we used the local sensitivity analysis to determine the sensitive parameters in the basin. According to Haan (2002), there are two types of sensitivity analysis: the local and global. In the local analysis, each parameter is changed one by one while keeping all other parameters unchanged, and its impact is measured on outputs. On the other hand, in the global analysis, a model is run with the initial values of parameters, the changes in parameters and output are measured, and the percentage effect of each parameter on the output is calculated to determine the sensitive parameters. The sensitivity analysis was carried out by changing each parameter by 10% each time (between -50% and $+50\%$) to observe the changes in simulated discharge. Three indicators such as peak flow (PF), total flow volume (TFV), and time to peak (TTP) were used to observe the effect of each parameter on discharge. The analysis showed the infiltration rate as the most sensitive parameter in the case of PF and TFV followed by Muskingum travel time. For TTP, Muskingum travel and time of concentration were found to be the most sensitive parameters compared with others. For the model calibration, we first changed each sensitive parameter by 5% to get roughly optimized parameters. Then, a built-in optimization technique in the model was utilized to determine the final optimized values for each parameter.

In this study, four commonly used indicators [i.e., coefficient of determination (R^2), Nash–Sutcliffe efficiency (E), root-mean-square error (RMSE), and percent volume deviation (PVD)] were used to check the model performance along with graphical plots, as in Mahmood and Jia (2019), García et al. (2008), Mahmood et al. (2016), Meenu et al. (2012), and Verma et al. (2010)

c. Discharge evolution in the twenty-first century

Since there were large biases in the RCMs' rainfall, a simple bias correction method, as described in Mahmood and Babel (2013), was used to correct rainfall from all RCMs under RCP2.6, RCP4.5, and RCP8.5. For this purpose, the biases were calculated for the period of 1971–2001 from the CRU and simulated rainfall, and then these biases were used to correct the future simulated rainfall. To verify the bias correction, the corrected and uncorrected climate data were forced

into HEC-HMS for the period of 2001–15 to simulate discharge. Then the simulated discharge (with and without correction) was compared with observed data at N'Djamena site, as shown in Fig. 2. This showed massive improvement after the correction of the RCMs' rainfall, and most importantly in the case of multimodel ensemble (MME), where observed discharge (thick black line) was well followed by MME (thick red line). After that, the corrected climate data for the period of 2021–2100 was used as input to HEC-HMS to simulate discharge at N'Djamena station on the Chari River under RCP2.6, RCP4.5, and RCP8.5. The simulated discharge (2021–2100) was divided into three periods: 2021–50 as a first time horizon (FTH), 2051–80 as a second time horizon (STH), and 2081–2100 as a third time horizon (TTH). Finally, the potential discharge changes were explored in these time horizons with respect to simulated flow for the baseline period (1971–2000). Thirty years of data is mostly used for a baseline period, as in Bodian et al. (2018) and Chilkoti et al. (2017), because a 30-yr period is considered long enough to describe current climate and to provide a good representation of dry, wet, cool, and warm periods (Benioff et al. 1996). Some studies such as Hu et al. (2015) and Wang et al. (2012) have used observed discharge data for the baseline period to determine the future discharge changes. However, it is recommended to use the simulated discharge for the baseline period to overcome any biases between observed and simulated discharge, which are observed during the calibration and validation process (Mahmood and Jia 2019).

d. Spectral analysis

Spectral analysis is a sophisticated technique, which is mostly applied to predict chaotic time series, such as rainfall, instead of using simple time series analysis such as moving average and autoregressive (Ehrendorfer 2011). In addition, it is also a reasonably fast and requires less computational requirements as compared to weather forecast models and climate models. Thus, in the present study, a spectral analysis and harmonic regression model were applied to predict discharge time series in the basin. For a time series Y_t having different components such as periodic, mean, and white noise, the harmonic regression model (HRM) can be formulated as below, as in Grzesica and Więcek (2016) and Hintze (2007):

$$Y_t = \mu + R\cos(ft + d) + \epsilon_t,$$

where μ, R, f, d, and ϵ_t represent the mean of time series, the amplitude of wave, the frequency of periodic variation, horizontal offset (phase), and white noise,
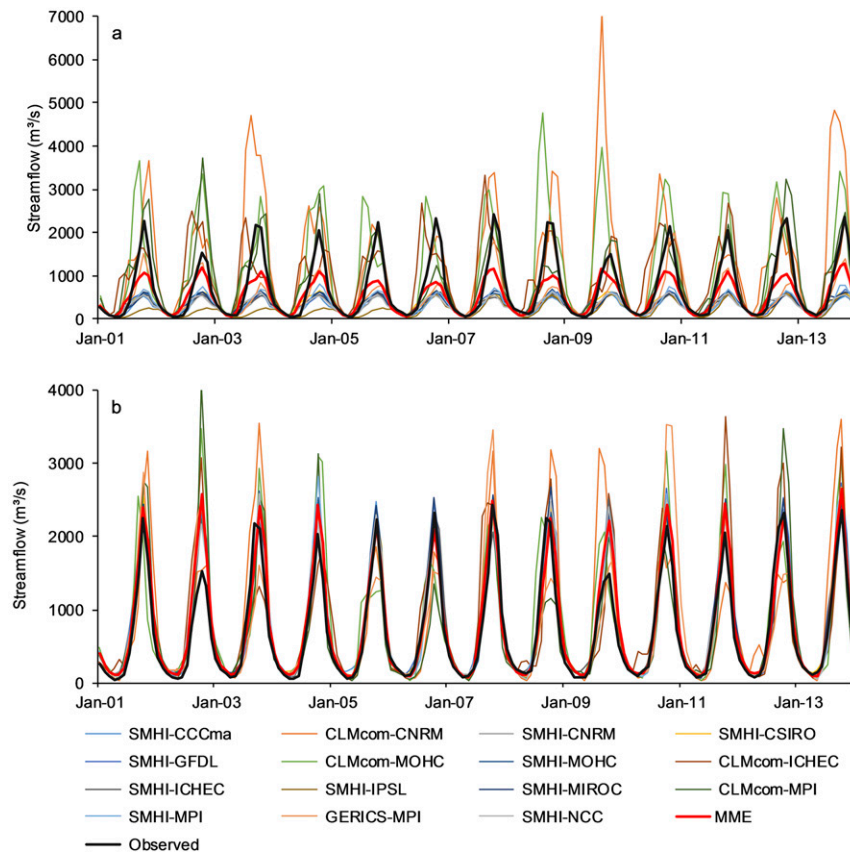
FIG. 2. Comparison of simulated discharge by (a) uncorrected and (b) corrected rainfall of the RCMs under RCP4.5 against the observed discharge at the N'Djamena site on the Chari River.

respectively, in a time series. The changes in *d* shifts the starting position of cycle. Finally, *t* represents the time period of observation (*t* = 1, 2, 3, . . . , *N*). To capture the fluctuations in a time series, the summation of several sinusoidal waves of different frequencies are required.

In the case of strong trend in a time series especially temperature and rainfall, either we incorporate a trend term into the HRM or we remove it from a time series to make it stationary. In the present study, the trend term (mt) was added in the HRM, as in Hintze (2007). After rearranging Eq. (1), the final HRM with the sum of *k* frequencies was formulated as below:

$$Y_t = \mu + \text{mt} + \sum_{j=1}^{k} a_j \cos(f_j t) + \sum_{j=1}^{k} b_j \sin(f_j t) + \epsilon_t,$$

where a_j and b_j (*j* = 1, 2, 3, . . . , *k*) are regression parameters of the HRM, which are estimated by fitting the model into a time series. Then these parameters are used in prediction process. In this approach, the most

critical process is to determine a set of wavelengths (or frequencies) because these frequencies define the cyclic behavior of a time series. For this purpose, a periodogram plot is created by using the spectral analysis (Fourier analysis). In spectral analysis, the cyclic behavior of a time series is converted into number of frequencies, which are shown by a periodogram, as shown Fig. 3. The frequencies of higher values have higher importance. For example, in Fig. 3, the 1.8 frequency has the highest value among other frequencies and has highest importance. In this way, a set of frequencies are chosen from the periodogram and incorporated into the HRM to generate a time series, which best match to the observed time series. More detail about the HRM and spectral analysis is given in Balıbey and Türkyılmaz (2015), Grzesica and Więcek (2016), Hintze (2007), Kozłowski et al. (2018), Mahmood and Jia (2019), and Yang and Lu (2011).

This whole process was performed on 37 monthly rainfall time series extracted from the CRU datasets. The prediction model HRM was fitted to these time series for the period of 1951–2015 for each time series.
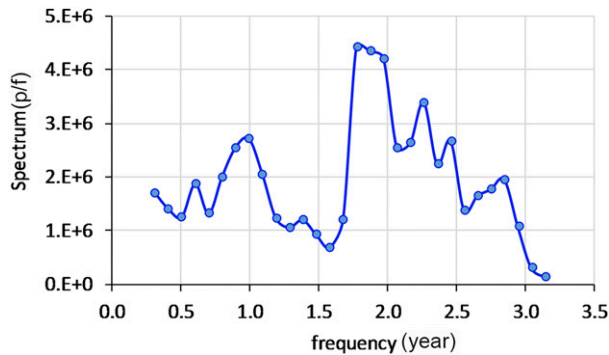
FIG. 3. Periodogram of rainfall of a subbasin (w1000) in the Chari River basin. Here *p/f* means power per frequency.

After the successful model fitting, the model was used to generate rainfall for the next two decades (2016–35), which was used as an input to hydrological model (HEC-HMS) to assess predicted discharge changes in the basin. Since HEC-HMS requires daily meteorological inputs (as a maximum time interval) to simulate discharge, the monthly CRU and generated data by the HRM were converted into daily data by using the Monthly to Daily Weather Convertor (MODAWEC) model (Liu et al. 2009). MODAWEC converts monthly rainfall and temperature to daily values while it preserves the monthly total rainfall and monthly average temperature. For rainfall disaggregation, a first-order Markov chain is applied to define whether a day is wet or dry. Markov chain models are based on transitional probability matrices of various time steps. Here, we assume that rainfall occurrence follows a two-state (wet or dry) transition probability: 1) the probability that a wet day comes after a dry day and 2) the probability of a wet day following a wet day. So the probability of rainfall occurrence is conditioned on the dry or wet status of the previous day. In the case of a wet day, a modified exponential distribution is applied to give initial estimation of daily rainfall amount. However, the final daily rainfall is obtained by modifying the initial approximations based on the given amount of monthly rainfall. The mathematical detail is given in Liu et al. (2009) for both rainfall and temperature disaggregation.

4. Results

a. Calibration and validation of HEC-HMS

The performance indicators (i.e., E, R^2, PVD, and RMSE) calculated from monthly simulated discharge and observed discharge at three hydrometric stations for both calibration and validation are described in Table 2. The E and R^2 values ranging from 0.93 to 0.98 during calibration and from 0.77 to 0.90 during validation showed that the model well captured the variations of observed discharge on all three sites. The PVD values varied from −0.2% to 13% during calibration and from −0.4% to 20% during validation. On the other hand, annual RMSE values were less than $60\,m^3\,s^{-1}$ during calibration and validation except at Bongor. According to Van Liew and Garbrecht (2003), E values greater than 0.75 are considered very good results and the values between 0.36 and 0.75 are referred to be satisfactory depending upon the objectives of the study. So our results are in the acceptable range and well comparable with Nkiaka et al. (2018) in the Logone River basin at Bongor and Coe and Foley (2001) and Gao et al. (2011) in the CRB at N'Djamena. They showed E values ranging from 0.64 to 0.78 and R^2 from 0.65 to 0.88.

The graphical presentation of results is another important visual tool for the evaluation of model performance subjectively and qualitatively. Therefore, the simulated discharge was plotted against the observed discharge to visualize the performance of the developed model at three gauges in the basin and is shown in Fig. 4. The simulated discharge followed well the observed discharge at all three sites, except in 2007, 2008, and 2014 at N'Djamena, where model underestimated during high flow months, and in 2009 at N'Djamena and 2005 at Sarh, where it overestimated in high flow months. We have discussed above that the model showed a higher value of PVD (20%) at Sarh, which was mostly due to the well overestimation of the model during the year 2005. In addition, this can be due to observed discharge because quality of discharge measurements is not high in the regions, as discussed in Stanzel et al. (2018) for different river basins in West Africa. Figure 4 clearly shows that the model's simulated discharge is well in

TABLE 2. Statistical indicators to evaluate the performance of HEC-HMS.

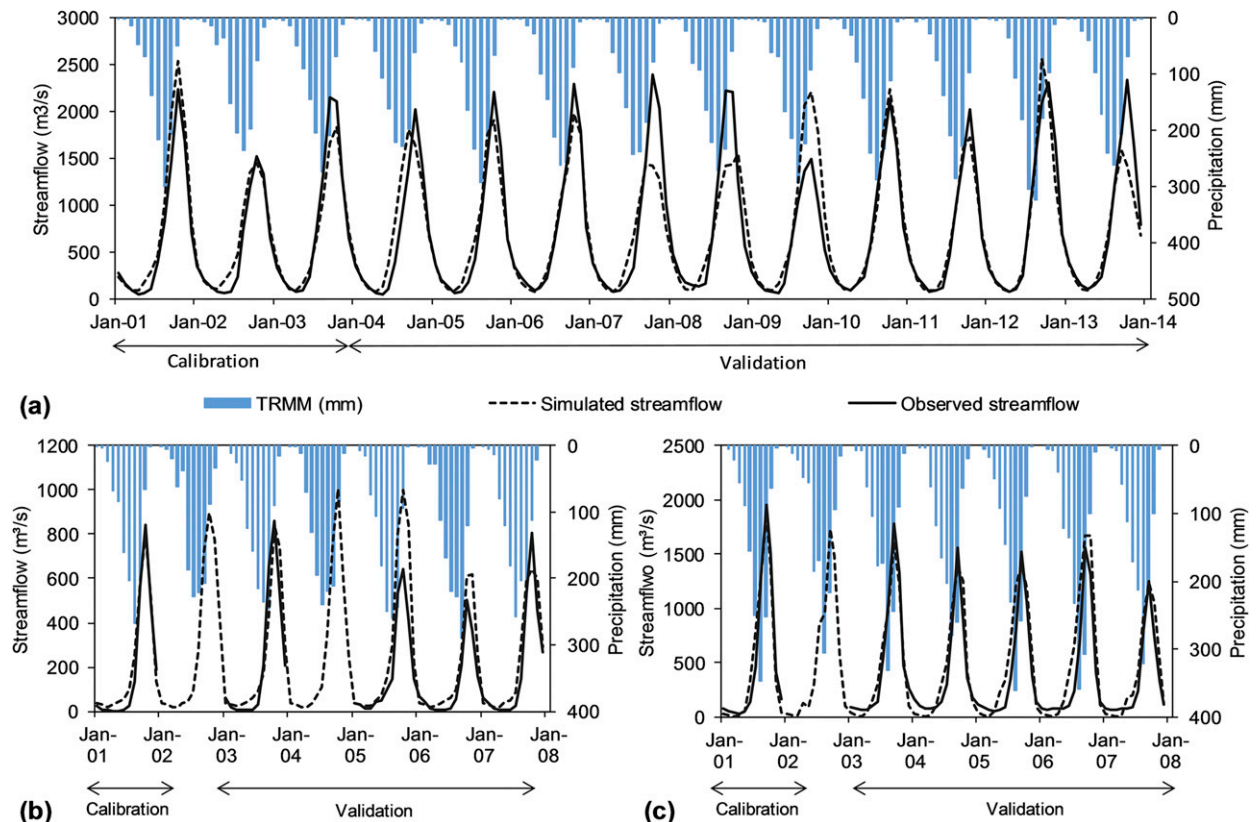| Indicators	Calibration			Validation		
	N'Djamena	Sarh	Bongor	N'Djamena	Sarh	Bongor
E	0.93	0.98	0.96	0.85	0.77	0.86
R^2	0.94	0.98	0.96	0.85	0.85	0.90
D (%)	7.7	12.7	−0.2	−0.4	20.4	14.8
Annual RMSE ($m^3\,s^{-1}$)	58.8	50.7	130	49.1	35.2	45.4

FIG. 4. Calibration and validation of hydrologic model at the (a) N'Djamena, (b) Sarh, and (c) Bongor hydrometric stations on the Chari River.

accordance with the TRMM rainfall annual cycle. Since the objective of the present study was to explore mean changes for longer period (e.g., 10-, 20-, and 30-yr means) relative to the baseline period, the model performance was well within the acceptable range according to qualitative (plots) and quantitative measures (indicators).

b. Evaluation of harmonic regression model

Correlation coefficient R^2, RMSE, and percent error in mean values E_σ were obtained from CRU and predicted rainfall time series for the fitted period (1951–2015) and are described in Table 3. It was noted that an average value of R^2 was 0.94 and 0.82 and an average value of RMSE was 6.3 mm month^{-1} and 45.7 mm yr^{-1} for monthly and annual rainfall time series, respectively. In the case of E_σ, an average value was −0.9% for both monthly and annual time series. These results show that the model performed reasonably well during verification, especially in the case of mean values. In addition to quantitative assessment, the simulated monthly, annual, and mean monthly rainfall (average of all 37 predicted time series) were plotted against the CRU rainfall for the fitted period (Figs. 5a–c)

to evaluate the model on graphical basis. In all three cases, the fitted model well captured the variations of the CRU time series. So the model can be used to predict the future discharge with high confidence.

c. Projected discharge changes under RCPs

1) LOW, HIGH, AND ANNUAL FLOW CHANGES

Table 4 describes changes in low, high, and annual flows for the period of 2021–50 (FTH), 2051–80 (STH), and 2081–2100 (TTH) with respect to the baseline period (1971–2000) at N'Djamena in the CRB. Low flow was calculated by taking an average of low flow months (December–July), which is a dry and premonsoon

TABLE 3. Statistical indicators for the evaluation of the harmonic regression model for the fitting period (1951–2015) on monthly and annual temporal resolution.

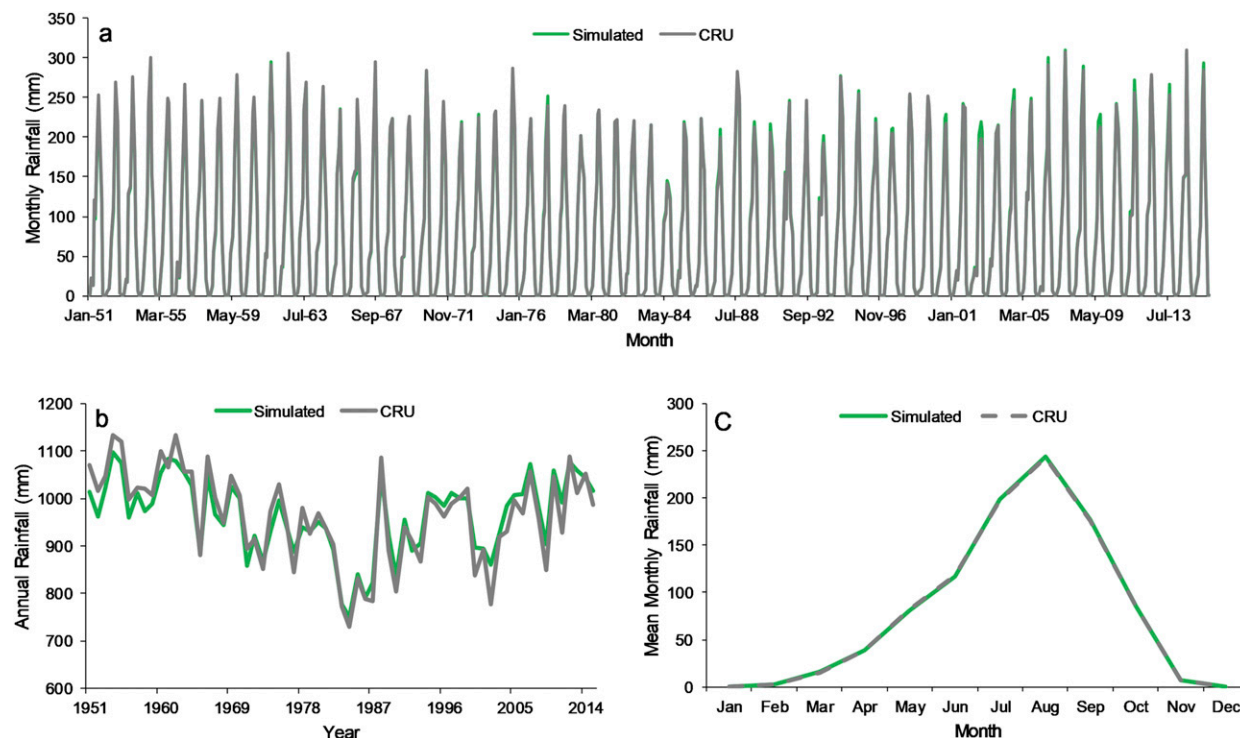| Indicator	Monthly		Annual	
	Average	Range	Average	Range
R^2	0.94	(0.91–0.98)	0.82	(0.67–0.90)
RMSE	6.3	(4.70–8.90)	45.7	(30.1–66.6)
E_σ (%)	−0.9	(−1.7 to −0.2)	−0.9	(−1.7 to −0.2)

FIG. 5. Comparison of monthly, annual, and mean monthly simulated rainfall and CRU rainfall for the fitting period (1951–2015).

season, and high flow was calculated by an average of high flow months (August–November), which is the monsoon season in the basin. These flow changes were calculated for all RCMs and their ensemble (MME). Instead of showing the changes in discharge for each model, we showed the changes in the form of range and MME. Before interpreting the results, analysis of variance (ANOVA) was used to find out whether the RCP datasets were different from each other or not.

In Table 4, the p value less than 0.05 shows statistically significant difference between RCPs. The results showed that RCPs datasets for all three horizons were statistically different except in the case of low flow in the third horizon. Since the RCPs datasets (low, high, and annual data) were statistical different, we described all RCPs separately. Under MME-RCP2.6 (ensemble of RCMs under RCP2.6), low, high, and annual flows were projected to decrease by 1.8%–3.1% in all time horizons

TABLE 4. Projected streamflow changes (%) in the Chari River basin at the N'Djamena hydrometric station using the multimodel ensemble (MME) of RCMs and the range of RCMs under RCPs. The bold number shows a statistically nonsignificant difference between the three RCP datasets.

	RCP2.6		RCP4.5		RCP8.5		
	MME	Range	MME	Range	MME	Range	p value
2021–50							
Low flow	−3.1	(−20 to 7)	−1.6	(−5 to 17)	0.6	(−7 to 30)	0.000 18
High flow	0.7	(−19 to 17)	3.7	(−1 to 17)	5.3	(−12 to 26)	0.000 59
Annual	−1.8	(−19 to 10)	0.2	(−4 to 17)	2.1	(−9 to 28)	0.000 00
2051–80							
Low flow	−3.1	(−21 to 10)	−3.3	(−7 to 26)	−0.8	(−7 to 39)	0.044 19
High flow	−2.4	(−31 to 11)	4.0	(−5 to 28)	8.3	(−12 to 49)	0.000 00
Annual	−2.9	(−25 to 11)	−0.9	(−7 to 27)	2.3	(−9 to 42)	0.000 00
2081–2100							
Low flow	**−3.0**	**(−21 to 9)**	**−2.2**	**(−8 to 38)**	**−2.8**	**(−10 to 46)**	**0.480 98**
Peak flow	−2.9	(−23 to 11)	6.6	(−3 to 36)	9.9	(−20 to 67)	0.000 00
Annual	−3.0	(−21 to 10)	0.8	(−6 to 37)	1.4	(−13 to 53)	0.000 05

except high flow in the FTH, where high flow was projected to increase by 0.7%. However, the changes in all flows ranged between −31% and 17% for all three horizons, showing large uncertainties in the projected changes. It was also observed that uncertainty in high flow was larger than low flow. Under MME-RCP4.5, low flow is projected to decrease by 1.6%–3.3% while high flow was projected to increase in the future by 4.0%– 6.6% in all three time horizons. In the case of annual flow, small positive changes were calculated in the FTH (0.2%) and TTH (0.8%) while negative change in the STH (−0.9%). On the other hand, flow changes (low, high, annual) varied from −5% to 17% in the FTH, from −7% to 28% in the STH, and from −8% to 38% in the TTH, showing the uncertainties in the results. It was also observed that uncertainties increased from the FTH to the TTH. This shows that the results for the far future can be more uncertain and less reliable. Under MME-RCP8.5, low flow was projected to increase in the FTH (0.6%) while projected to decrease in the STH (−0.8%) and TTH (−2.8%), indicating a pattern of decreasing low flow from the first to last time period. In contrast, an increasing pattern was projected in high flow along the time, with 5.3%, 8.3%, and 9.9% in the FTH, STH, and TTH, respectively. Annual flow was also projected to increase but there was no linear pattern of decrease or increase. Under RCP8.5, uncertainties were even greater than RCP4.5 and RCP2.6. For example, all types of flow varied from −12% to 30% in the FTH, from −12% to 49% in the STH, and from −20% to 67% in the TTH.

In general, low flow was projected to decrease by 0.8%–3.3% in all three horizons under all three RCPs (except under RCP8.5 in the FTH), and most reduction was observed under RCP4.5 in the STH. By contrast, high flow was predicted to increase by 0.7%–9.9% under all RCPs in all the three horizons (except under RCP2.6 in the STH and TTH, where flow decreased). Similar to high flow, annual flow will increase by 0.2%– 2.3% under RCP4.5 and RCP8.5 (except under RCP4.5 in the STH) while it will decrease under RCP2.6 in all three horizons.

2) DISCHARGE EVOLUTION IN THE TWENTY-FIRST CENTURY

To explore the evolution of discharge in the twenty-first century, we plotted the annul MME simulated flow under RCPs for the period of 2006–2100 along with MME historic flow, the range of MME flow, and observed discharge at the N'Djamena gauge on the Chari River, as shown in Fig. 6. The annual anomalies in the projected MME flow (2006–2100) with respect to the historic MME flow (1971–2000) were also plotted to explore evolution of annual changes for the period of 2006–2100 (Fig. 6, small anomaly plots). Under MME-RCP2.6, discharge almost remained stable throughout the twenty-first century (Fig. 6a). However, anomaly plot showed more negative spikes than positive, resulting in a little decrease (about 2%) in annual discharge, which will remain constant throughout the projected period (black dotted trend line). Under MME-RCP4.5, the projected discharge showed a gradual increase toward the end of projected period, with 0.12% increase per year (Fig. 6b). This means discharge may increase by about 5.5% at midcentury and 11% at the end of this century. The similar evolution of annual discharge was projected under MME-RCP8.5. Nonetheless, the linear trend line showed a stronger increasing trend than MME-RCP4.5, even more than a double increase per year (0.29%) relative to MME-RCP4.5 (0.12% yr^{-1}) (Fig. 6c). With this rate, discharge may increase by about 12% at midcentury and about 27% at the end of the projected period. It was also observed that if projected discharge follows the upper end of the range of MME under RCP4.5 and RCP8.5, then the discharge may reach the discharge of the Chari River that existed in 1950s and 1960s, toward the end of the twenty-first century.

d. Predicted discharge changes in next two decades

Table 5 describes the predicted changes in low, high, and annual flows using the HRM (prediction model) and using multimodel approach under RCP2.6, RCP4.5, and RCP8.5. According to the HRM, low, high, and annual flows were predicted to decrease in the both decades (i.e., 2016–25 and 2026–35). In both decades, high flow was predicted to decrease more than low flows, with 5.8% in 2016–25 and 11.3% in 2026–35. On the whole, annual flow will decline by 3.0% in 2016–25 and 5.9% in 2026–35. It was also observed that reduction in flow was greater in the second decade. This means the water resources of the basin can be at high risk in the coming years. Similar to the HRM, under MME-RCP2.6, low and annual flow will decrease but, in contrast to the HRM, high flow will increase in both decades relative to the baseline period. However, in the second decade, high flow will decrease from 1.3% (2016–25) to 0.1% (2026–35), very similar to the prediction model. It was noted that even if the climate follows RCP2.6 (which is considered as the best pathway to limit the emission of GHG and results in limiting the climate change) the water resources of the basin will be at high risk. Nonetheless, under MME-RCP4.5 and MME-RCP8.5, the stream was projected to increase in both decades except for low flow under RCP4.5 in the second decade. It was also observed that the projected positive
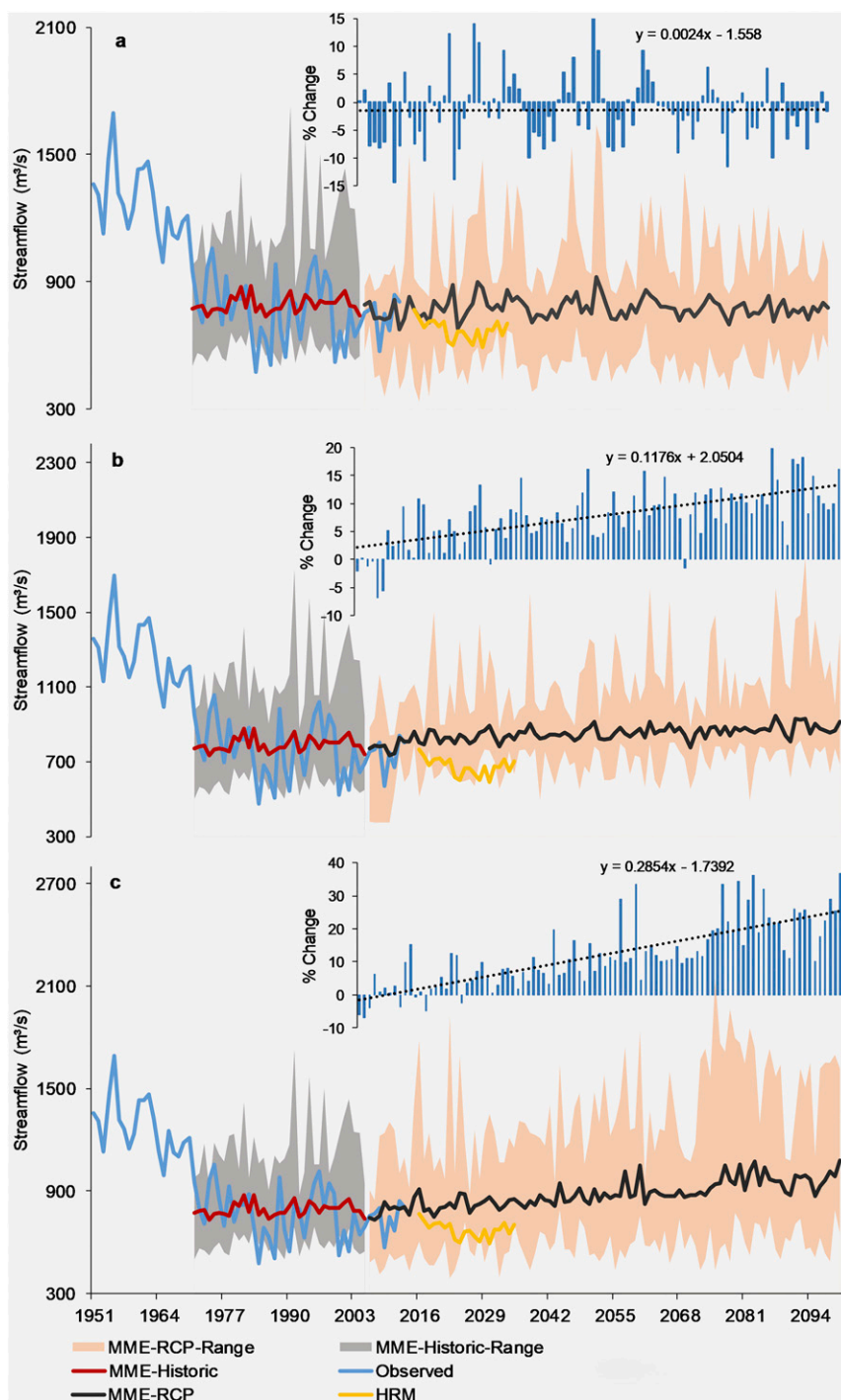
FIG. 6. Streamflow evolution in the Chari River basin at N'Djamena in the twenty-first century under (a) RCP2.6, (b) RCP4.5, and (c) RCP8.5. The black line is the multimodel ensemble (MME) of all RCMs, the shaded area shows the range of MME for historic and RCPs, the red line is MME of RCMs for historic period (1971–2000), the yellow line is the predicted flow by harmonic regression model, and the bar chart is the annual anomaly with respect to mean of MME historic.

TABLE 5. Anticipated streamflow changes (%) for the next two decades (2016–35) at the N'Djamena gauge on the Chari River using the harmonic regression model and MME of RCMs. The bold number shows a statistically significant difference between the harmonic regression model and RCPs ($\alpha = 0.05$).

	Harmonic regression	MME-RCP26	MME-RCP45	MME-RCP85
2016–25				
Low flow	−1.6	−3.5	**3.8**	1.0
High flow	−5.8	**1.3**	**6.4**	**4.9**
Annual	−3.0	−1.9	**4.7**	**2.3**
2025–35				
Low flow	−3.2	−2.4	−1.4	0.8
High flow	−11.3	**0.1**	**4.5**	**4.6**
Annual	−5.9	−1.6	**0.6**	**2.1**

changes were higher in the first decade than the second. Overall, annual discharge is expected to increase by 4.7% (2016–25) and 0.6% (2026–35) under MME-RCP4.5 and 2.3% (2016–25) and 2.1% (2026–35) under MME-RCP8.5 in the basin. The projected changes in high flow were almost similar in both decades under MME-RCP4.5 and MME-RCP8.5, with an average of 5%.

Since the differences in changes (low, high, and annual flows) between HRM and RCPs were small, it was necessary to explore whether these differences were statistically significant or not. For this purpose, we applied a *t* test between the values of HRM and RCPs (one by one) at the 5% significance level. The results showed that low and annual flow changes under MME-RCP2.6 were not significantly different from HRM. However, the flow changes under MME-RCP4.5 and MME-RCP8.5 were mostly significantly different from HRM. It was expected that for a short time horizon (2016–35), the predicted and projected changes should be similar. Nonetheless, Fig. 6 shows that predicted changes by HRM were within the lower range of RCPs. From the above results, it is quite difficult to conclude that either the flow will increase or decrease, under MME-RCPs and HRM because MME-RCP2.6 shows a decrease in flow while MME-RCP4.5 and MME-RCP8.5 show an increase in flow. So it is better to give a range of changes. According to the results, the annual flow can change from −3% to 4.5% in the first decade and from −5.9% to 2.1% in the second decade.

5. Discussion

a. Evaluation of results under the light of previous studies

Generally, the discharge will decrease under MME-RCP2.6 as well as the HRM and increase under MME-RCP4.5 and MME-RCP8.5 in the next two decades (2016–35) as well as in the twenty-first century. Since there is a lack of studies in the CRB on this topic, the results were evaluated with some other studies conducted around the basin. The similar positive changes in runoff has been reported by Mahé et al. (2008) over the LCB in the twenty-first century under the A2 scenario, which is also high emission scenario like RCP8.5. In addition, Basheer et al. (2016) and Stanzel et al. (2018) also explored positive changes in discharge in the Dinder River basin, Sudan (located to the east of the CRB) and Côte d'Ivoire, Liberia, Sierra Leone, and Guinea (located around the CRB) under RCP4.5 and RCP8.5. Roudier et al. (2014) reviewed different studies to explore the runoff changes under a changing climate over West Africa. They conclude that the future tendency in discharge evolution is, on the whole, very uncertain. They showed an overall increase of 5.2% over West Africa.

The main factors of changes in discharge (i.e., increase or decrease) can be the changes in rainfall and temperature. Recently, Mahmood et al. (2019) predicted increase in temperature and decrease in precipitation for the next 20 years over the LCB. These changes in climate can be the major causes of decreasing discharge in the Chari River. Another main factor of decreasing discharge can be the human interventions in the basin. Coe and Foley (2001) explored that climate change and human activities have almost equal impact on the decreasing discharge in the Chari River. However, Mahmood and Jia (2019) showed that human activities have dominant impacts on the decreasing discharge in the Chari River. They determined a 40% reduction in the discharge of the Chari River was due to both climate change and human activities, out of which 66% was quantified due to human intervention and 34% due to climate variability. So the projected decreasing discharge in the basin can definitely be due to climate variability and human activities. So both factors (climate and human) must be considered equally when planning water resources of the Chari River. Some other studies, such as Buontempo (2010), Engelbrecht et al. (2015), Niang et al. (2014), Sarr (2012), Serdeczny et al. (2017), and Sylla et al. (2016), have also projected an increase in temperature in different parts of Africa, especially over the Sahel, under RCP4.5 and RCP8.5. According to IPCC (2007), global warming would be more intense in the future over Africa rather than the rest of the world, which can greatly impact the discharge of the Chari River. Different studies showed projected rainfall changes in different parts of Africa, which can be discussed here to indirectly evaluate the results of the present study. For example, Sultan et al. (2014)

projected an increase in annual rainfall over the Central Sahel under RCP8.5, Vizy et al. (2013) showed an increase in summer rainfall over the Sahel region under RCP8.5, and Sylla et al. (2010) projected drier conditions over the Sahel region and wetter over orographic regions in the twenty-first century. According to Niang et al. (2014), annual rainfall is *likely* to increase in Central and Eastern Africa in the beginning of the mid-twenty-first century under RCP8.5. Most of the above studies, directly or indirectly, are well in agreement with the results of the present study.

b. Limitations and sources of uncertainties

It is also of worth to discuss the limitations and uncertainties in the present study. Since observed data are so sparse and not of good quality, we used the CRU data in the prediction analysis and the TRMM data in the calibration of hydrological model. In Mahmood and Jia (2019), the CRU climatic data were evaluated with some good quality observed data, and RMSE values of 0.6°–0.97°C for temperature and 26–44 mm month^{-1} for precipitation were explored, which is the first main source of uncertainties in the results. According to Bastola and François (2012), the CRU precipitation was also underestimated in humid regions of the LCB, while overestimated in semiarid and arid regions. This source of uncertainty can be minimized by using a bias correction technique, but the availability of good quality observed data is the main limitation in the basin.

The second source can be simplification of hydrologic processes in a hydrological model. For example, we used a single-layer loss calculation method, which cannot present completely the soil moisture losses as a complex and sophisticated loss method such as continuous soil moisture accounting method can do. However, for a sophisticated loss method, much more data are required rather than a simple method, which is another limitation in the present study.

The third source of uncertainty can be the conversion of monthly predicted temperature and precipitation to daily data. In the prediction model, we used monthly CRU data for model fitting and generated the monthly data for the next 20 years, and then these predicted data were converted into daily format as the requirement of hydrologic model. According to Zhang et al. (2016), the estimation of parameters during the calibration process can be another source of uncertainty because it is impossible to determine the exact parameters of the study site. Last but not least, the future projection under different emission scenarios is itself one of the biggest uncertainties because nobody exactly knows how the climate will change in the future.

In general, the sources of uncertainties can be categorized into four main groups (Renard et al. 2010): 1) input uncertainty, 2) output uncertainty, 3) model uncertainty, and 4) parametric uncertainty.

6. Conclusions

Since the water resources of the Chari River located in the Lake Chad basin are highly vulnerable to climate change, it is of great importance to have knowledge of how the discharge in the river will be in the future. Therefore, in the present study, the predicted discharge changes using a combination of spectral analysis and the harmonic regression model were revealed for the next two decades (2016–35), and a multimodel approach was used to determine the projected discharge changes under IPCC emission scenarios (i.e., RCP2.6, RCP4.5, and RCP8.5) for the period of 2021–2100. Since observed data are so sparse in the basin, the TRMM and CRU climatic data were used in the analysis of the study. The downscaled climatic data of 11 GCMs driven by 3 RCMs under RCPs were obtained from CORDEX for the period of 1971–2000 and 2021–2100. The projected discharge changes were calculated for three time horizons: 2021–50 as the first time horizon (FTH), 2051–80 as the second time horizon (STH), and 2081–2100 as the third time horizon (TTH) with respect to the simulated historical period (1971–2000). The key findings obtained from the present study are as follows:

- Under MME-RCP2.6, low, high, and annual flows were projected to decrease in all three horizons except high flow in the FTH, and the decrease in high and annual flows were stronger in the TTH followed by the STH.
- Under MME-RCP4.5 and MME-RCP8.5, high and annual flows were projected to increase while low flows were projected to decrease in all three horizons.
- High flow (72% of annual flow) will increase if the climate follows RCP4.5 and RCP8.5, and the increase will be stronger with passage of time. In contrast, it will decrease under RCP2.6, and decrease will be stronger toward the end of the twenty-first century.
- Prediction analysis shows a decrease in low, high, and annual flows in both decades (2016–25 and 2026–35) and even stronger in the second decades.
- In the next two decades (2016–25 and 2026–35), low and annual flow will decrease and high flow will increase under RCP2.6. In contrast, low, high, and annual flows were projected to increase under RCP4.5 and 8.5 except low flow under RCP4.5 in the second decades.
- Evolution of annual flow shows increasing trends in annual flow from 2006 to 2100 under RCP4.5 and

RCP8.5 while there was a very light decrease in annual flow under RCP2.6 (about 2% for 2021–2100).

From the above finding, it can be concluded that streamflow will increase if the climate of the basin will follow RCP4.5 and RCP8.5 and decrease if the climate will follow RCP2.6, for long term projection (2021–2100). For short period (2016–35), the flow will decrease according to prediction and MME-RCP2.6 and increase according to MME-RCP4.5 and MME-RCP8.5. Because there is a big uncertainty in short period results, it is recommended to use range of flow changes between the HRM and RCPs' results. The results of present study may be helpful to water resources managers and planner to plan the water resources on a seasonal and annual basis and to policy makers for advising some suitable adaptation and mitigation policies to cope with anticipated environmental changes. However, further studies are suggested to include observed climate data and more sophisticated loss methods (which include losses from canopy interception, surface and soil, and ground layers), and baseflow methods, such as the linear reservoir method, in hydrologic modeling. In addition, canopy interception and depression storage can also be included in a distributed model. Furthermore, as we used a multimodel approach for RCMs, multi–time series techniques can be used for prediction of rainfall to count uncertainties in prediction methods.

REFERENCES

Abramowitz, G., and Coauthors, 2019: ESD Reviews: Model dependence in multi-model climate ensembles: Weighting, subselection and out-of-sample testing. *Earth Syst. Dynam.*, **10**, 91–105, https://doi.org/10.5194/esd-10-91-2019.

Ahbari, A., L. Stour, A. Agoumi, and N. Serhir, 2018: Estimation of initial values of the HMS model parameters: Application to the basin of Bin El Ouidane (Azilal, Morocco). *J. Mater. Environ. Sci.*, **9**, 305–317, https://doi.org/10.26872/jmes.2018.9.1.34.

Ahmadalipour, A., A. Rana, H. Moradkhani, and A. Sharma, 2017: Multi-criteria evaluation of CMIP5 GCMs for climate change impact analysis. *Theor. Appl. Climatol.*, **128**, 71–87, https://doi.org/10.1007/s00704-015-1695-4.

Aich, V., and Coauthors, 2014: Comparing impacts of climate change on streamflow in four large African river basins. *Hydrol. Earth Syst. Sci.*, **18**, 1305–1321, https://doi.org/10.5194/hess-18-1305-2014.

Balıbey, M., and S. Türkyılmaz, 2015: A time series approach for precipitation in Turkey. *Gazi Univ. J. Sci.*, **28**, 549–559.

Basheer, A. K., H. Lu, A. Omer, A. B. Ali, and A. M. S. Abdelgader, 2016: Impacts of climate change under CMIP5 RCP scenarios on the streamflow in the Dinder River and ecosystem habitats in Dinder National Park, Sudan. *Hydrol. Earth Syst. Sci.*, **20**, 1331–1353, https://doi.org/10.5194/hess-20-1331-2016.

Bastola, S., and D. François, 2012: Temporal extension of meteorological records for hydrological modelling of Lake Chad Basin (Africa) using satellite rainfall data and reanalysis datasets. *Meteor. Appl.*, **19**, 54–70, https://doi.org/10.1002/met.257.

Benioff, R., S. Guill, and J. Lee, Eds., 1996: *Vulnerability and Adaptation Assessments: An International Handbook.* Environmental Science and Technology Library, Vol. 7, Kluwer Academic, 564 pp.

Bodian, A., A. Dezetter, L. Diop, A. Deme, K. Djaman, and A. Diop, 2018: Future climate change impacts on streamflows of two main West Africa River basins: Senegal and Gambia. *Hydrology*, **5**, 21, https://doi.org/10.3390/hydrology5010021.

Buma, W., S.-I. Lee, and J. Seo, 2016: Hydrological evaluation of Lake Chad basin using space borne and hydrological model observations. *Water*, **8**, 205, https://doi.org/10.3390/w8050205.

Buontempo, C., 2010: Sahelian climate: Part, current, projections. Met Office Rep., 20 pp., https://www.oecd.org/swac/publications/47092928.pdf.

Chilkoti, V., T. Bolisetti, and R. Balachandar, 2017: Climate change impact assessment on hydropower generation using multi-model climate ensemble. *Renew. Energy*, **109**, 510–517, https://doi.org/10.1016/j.renene.2017.02.041.

Coe, M. T., and J. A. Foley, 2001: Human and natural impacts on the water resources of the Lake Chad basin. *J. Geophys. Res.*, **106**, 3349–3356, https://doi.org/10.1029/2000JD900587.

Collischonn, B., W. Collischonn, and C. E. M. Tucci, 2008: Daily hydrological modeling in the Amazon basin using TRMM rainfall estimates. *J. Hydrol.*, **360**, 207–216, https://doi.org/10.1016/j.jhydrol.2008.07.032.

Diallo, I., M. B. Sylla, F. Giorgi, A. T. Gaye, and M. Camara, 2012: Multimodel GCM-RCM ensemble-based projections of temperature and precipitation over West Africa for the early 21st century. *Int. J. Geophys.*, **2012**, 972896, https://doi.org/10.1155/2012/972896.

Ehrendorfer, M., 2011: *Spectral Numerical Weather Prediction Models.* Society for Industrial and Applied Mathematics, 507 pp.

Endris, H. S., C. Lennard, B. Hewitson, A. Dosio, G. Nikulin, and H.-J. Panitz, 2016: Teleconnection responses in multi-GCM driven CORDEX RCMs over Eastern Africa. *Climate Dyn.*, **46**, 2821–2846, https://doi.org/10.1007/s00382-015-2734-7.

Engelbrecht, F., and Coauthors, 2015: Projections of rapidly rising surface temperatures over Africa under low mitigation. *Environ. Res. Lett.*, **10**, 085004, https://doi.org/10.1088/1748-9326/10/8/085004.

Feldman, A. D., 2000: Hydrological Modeling System HEC-HMS. USACE Technical Reference Manual, Rep. CPD-74B, 138 pp., https://www.hec.usace.army.mil/software/hec-hms/documentation/HEC-HMS_Technical%20Reference%20Manual_(CPD-74B).pdf.

Feng, G., S. Cobb, Z. Abdo, D. K. Fisher, Y. Ouyang, A. Adeli, and J. N. Jenkins, 2016: Trend analysis and forecast of

precipitation, reference evapotranspiration, and rainfall deficit in the Blackland Prairie of eastern Mississippi. *J. Appl. Meteor. Climatol.*, **55**, 1425–1439, https://doi.org/10.1175/JAMC-D-15-0265.1.

Gädeke, A., H. Hölzel, H. Koch, I. Pohle, and U. Grünewald, 2014: Analysis of uncertainties in the hydrological response of a model-based climate change impact assessment in a sub-catchment of the Spree River, Germany. *Hydrol. Processes*, **28**, 3978–3998, https://doi.org/10.1002/hyp.9933.

Gao, H., T. J. Bohn, E. Podest, K. C. McDonald, and D. P. Lettenmaier, 2011: On the causes of the shrinking of Lake Chad. *Environ. Res. Lett.*, **6**, 034021, https://doi.org/10.1088/1748-9326/6/3/034021.

García, A., A. Sainz, J. A. Revilla, C. Álvarez, J. A. Juanes, and A. Puente, 2008: Surface water resources assessment in scarcely gauged basins in the north of Spain. *J. Hydrol.*, **356**, 312–326, https://doi.org/10.1016/j.jhydrol.2008.04.019.

Ghoraba, S. M., 2015: Hydrological modeling of the Simly Dam watershed (Pakistan) using GIS and SWAT model. *Alexandria Eng. J.*, **54**, 583–594, https://doi.org/10.1016/j.aej.2015.05.018.

Giorgi, F., 2005: Climate change prediction. *Climatic Change*, **73**, 239–265, https://doi.org/10.1007/s10584-005-6857-4.

Grzesica, D., and P. Więcek, 2016: Advanced forecasting methods based on spectral analysis. *Procedia Eng.*, **161**, 253–258, https://doi.org/10.1016/j.proeng.2016.08.546.

Gu, H.-h., Z.-b. Yu, C.-g. Yang, Q. Ju, B.-h. Lu, and C. Liang, 2010: Hydrological assessment of TRMM rainfall data over Yangtze River Basin. *Water Sci. Eng.*, **3**, 418–430, https://doi.org/10.3882/j.issn.1674-2370.2010.04.005.

Haan, C. T., 2002: *Statistical Methods in Hydrology*. 2nd ed. Wiley-Blackwell, 378 pp.

Haensler, A., F. Saeed, and D. Jacob, 2013: Assessing the robustness of projected precipitation changes over central Africa on the basis of a multitude of global and regional climate projections. *Climatic Change*, **121**, 349–363, https://doi.org/10.1007/s10584-013-0863-8.

Halwatura, D., and M. M. M. Najim, 2013: Application of the HEC-HMS model for runoff simulation in a tropical catchment. *Environ. Modell. Software*, **46**, 155–162, https://doi.org/10.1016/j.envsoft.2013.03.006.

Harris, I., P. D. Jones, T. J. Osborn, and D. H. Lister, 2014: Updated high-resolution grids of monthly climatic observations – the CRU TS3.10 Dataset. *Int. J. Climatol.*, **34**, 623–642, https://doi.org/10.1002/joc.3711.

He, Z., H. Hu, F. Tian, G. Ni, and Q. Hu, 2017: Correcting the TRMM rainfall product for hydrological modelling in sparsely-gauged mountainous basins. *Hydrol. Sci. J.*, **62**, 306–318, https://doi.org/10.1080/02626667.2016.1222532.

Hill, T., P. Lewicki, and P. Lewicki, 2006: *Statistics: Methods and Applications: A Comprehensive Reference for Science, Industry, and Data Mining*. StatSoft, 832 pp.

Hintze, J. L., 2007: User's guide I: Quick Start & Self Help, Introduction, Data, Tools, and Graphics. NCSS Statistical System, 629 pp., https://ncss-wpengine.netdna-ssl.com/wp-content/uploads/2012/09/NCSSUG1.pdf.

Hu, Z., L. Wang, Z. Wang, Y. Hong, and H. Zheng, 2015: Quantitative assessment of climate and human impacts on surface water resources in a typical semi-arid watershed in the middle reaches of the Yellow River from 1985 to 2006. *Int. J. Climatol.*, **35**, 97–113, https://doi.org/10.1002/joc.3965.

Hughes, D. A., 2006: Comparison of satellite rainfall data with observations from gauging station networks. *J. Hydrol.*, **327**, 399–410, https://doi.org/10.1016/j.jhydrol.2005.11.041.

IPCC, 2007: *Climate Change 2007: The Physical Science Basis*. Cambridge University Press, 996 pp.

Karambiri, H., S. G. García Galiano, J. D. Giraldo, H. Yacouba, B. Ibrahim, B. Barbier, and J. Polcher, 2011: Assessing the impact of climate variability and climate change on runoff in West Africa: The case of Senegal and Nakambe River basins. *Atmos. Sci. Lett.*, **12**, 109–115, https://doi.org/10.1002/asl.317.

Komble, M. D., B. Kostoingue, and A. Hamit, 2016: Report on the state of the Lake Chad Basin ecosystem. Lake Chad Basin Commission, 236 pp., http://www.cblt.org/sites/default/files/download_documents/report_on_the_state_of_the_lake_chad_basin_ecosystem.pdf.

Kozłowski, E., B. Kowalska, D. Kowalski, and D. Mazurkiewicz, 2018: Water demand forecasting by trend and harmonic analysis. *Arch. Civ. Mech. Eng.*, **18**, 140–148, https://doi.org/10.1016/j.acme.2017.05.006.

Landman, W. A., and A. Beraki, 2012: Multi-model forecast skill for mid-summer rainfall over southern Africa. *Int. J. Climatol.*, **32**, 303–314, https://doi.org/10.1002/joc.2273.

LCBC, 2011: Lake Chad: Mapping of the Lake Chad. Lake Chad Basin Commission, http://www.cblt.org/en/lake-chad.

Leblanc, M., J. Lemoalle, J. C. Bader, S. Tweed, and L. Mofor, 2011: Thermal remote sensing of water under flooded vegetation: New observations of inundation patterns for the 'Small' Lake Chad. *J. Hydrol.*, **404**, 87–98, https://doi.org/10.1016/j.jhydrol.2011.04.023.

Lemoalle, J., and G. Magrin, 2014: *Le développement du lac Tchad: Situation actuelle et futurs possibles* (*Development of Lake Chad: Current Situation and Possible Outcomes*). Institut de Recherche pour le Développement, 215 pp.

——, J.-C. Bader, M. Leblanc, and A. Sedick, 2012: Recent changes in Lake Chad: Observations, simulations and management options (1973–2011). *Global Planet. Change*, **80–81**, 247–254, https://doi.org/10.1016/j.gloplacha.2011.07.004.

Liu, J., J. R. Williams, X. Wang, and H. Yang, 2009: Using MODAWEC to generate daily weather data for the EPIC model. *Environ. Modell. Software*, **24**, 655–664, https://doi.org/10.1016/j.envsoft.2008.10.008.

Liu, X., F. M. Liu, X. X. Wang, X. D. Li, Y. Y. Fan, S. X. Cai, and T. Q. Ao, 2017: Combining rainfall data from rain gauges and TRMM in hydrological modelling of Laotian data-sparse basins. *Appl. Water Sci.*, **7**, 1487–1496, https://doi.org/10.1007/s13201-015-0330-y.

Losada, T., B. Rodríguez-Fonseca, S. Janicot, S. Gervois, F. Chauvin, and P. Ruti, 2010: A multi-model approach to the Atlantic Equatorial mode: Impact on the West African monsoon. *Climate Dyn.*, **35**, 29–43, https://doi.org/10.1007/s00382-009-0625-5.

Lyne, V., and M. Hollick, 1979: *Stochastic Time-Variable Rainfall-Runoff Modeling. Hydrology and Water Resources Symp.*, Perth, Australia, Institution of Engineers Australia, 89–92.

Mahé, G., and Coauthors, 2008: Climate and river runoff changes in West and Central Africa: Past variability and prediction of water resources for the 21st century. *XIII World Water Congress*, Montpellier, France, Internation Water Resouces Association, 13 pp.

Mahmood, R., and M. S. Babel, 2013: Evaluation of SDSM developed by annual and monthly sub-models for downscaling temperature and precipitation in the Jhelum basin, Pakistan and India. *Theor. Appl. Climatol.*, **113**, 27–44, https://doi.org/10.1007/s00704-012-0765-0.

——, and S. Jia, 2016: Assessment of impacts of climate change on the water resources of the transboundary Jhelum River Basin

of Pakistan and India. *Water*, **8**, 246, https://doi.org/10.3390/w8060246.

——, and ——, 2017: Spatial and temporal hydro-climatic trends in the transboundary Jhelum River basin. *J. Water Climate Change*, **8**, 423–440, https://doi.org/10.2166/wcc.2017.005.

——, and ——, 2019: Assessment of hydro-climatic trends and causes of dramatically declining stream flow to Lake Chad, Africa, using a hydrological approach. *Sci. Total Environ.*, **675**, 122–140, https://doi.org/10.1016/j.scitotenv.2019.04.219.

——, ——, and S. M. Babel, 2016: Potential impacts of climate change on water resources in the Kunhar River basin, Pakistan. *Water*, **8**, 23, https://doi.org/10.3390/w8010023.

——, ——, N. K. Tripathi, and S. Shrestha, 2018: Precipitation extended linear scaling method for correcting GCM precipitation and its evaluation and implication in the transboundary Jhelum River basin. *Atmosphere*, **9**, 160, https://doi.org/10.3390/atmos9050160.

——, ——, and W. Zhu, 2019: Analysis of climate variability, trends, and prediction in the most active parts of the Lake Chad basin, Africa. *Sci. Rep.*, **9**, 6317, https://doi.org/10.1038/s41598-019-42811-9.

McMahon, T. A., M. C. Peel, and D. J. Karoly, 2015: Assessment of precipitation and temperature data from CMIP3 global climate models for hydrologic simulation. *Hydrol. Earth Syst. Sci.*, **19**, 361–377, https://doi.org/10.5194/hess-19-361-2015.

Meenu, R., S. Rehana, and P. P. Mujumdar, 2012: Assessment of hydrologic impacts of climate change in Tunga-Bhadra River basin, India with HEC-HMS and SDSM. *Hydrol. Processes*, **27**, 1572–1589, https://doi.org/10.1002/hyp.9220.

Meng, J., L. Li, Z. Hao, J. Wang, and Q. Shao, 2014: Suitability of TRMM satellite rainfall in driving a distributed hydrological model in the source region of Yellow River. *J. Hydrol.*, **509**, 320–332, https://doi.org/10.1016/j.jhydrol.2013.11.049.

Miao, C., and Coauthors, 2014: Assessment of CMIP5 climate models and projected temperature changes over Northern Eurasia. *Environ. Res. Lett.*, **9**, 055007, https://doi.org/10.1088/1748-9326/9/5/055007.

Moss, R. H., and Coauthors, 2010: The next generation of scenarios for climate change research and assessment. *Nature*, **463**, 747, https://doi.org/10.1038/nature08823.

Niang, I., O. C. Ruppel, M. A. Abdrabo, A. Essel, C. Lennard, J. Padgham, and P. Urquhart, 2014: Africa. *Climate Change 2014: Impacts, Adaptation, and Vulnerability. Part B: Regional Aspects*, Cambridge University Press, 1199–1265.

Nikiema, P. M., B. Sylla Mouhamadou, K. Ogunjobi, I. Kebe, P. Gibba, and F. Giorgi, 2017: Multi-model CMIP5 and CORDEX simulations of historical summer temperature and precipitation variabilities over West Africa. *Int. J. Climatol.*, **37**, 2438–2450, https://doi.org/10.1002/joc.4856.

Nkiaka, E., N. R. Nawaz, and J. C. Lovett, 2018: Effect of single and multi-site calibration techniques on hydrological model performance, parameter estimation and predictive uncertainty: A case study in the Logone catchment, Lake Chad basin. *Stochastic Environ. Res. Risk Assess.*, **32**, 1665–1682, https://doi.org/10.1007/s00477-017-1466-0.

Nury, A. H., M. Koch, and M. J. B. Alam, 2013: Time series analysis and forecasting of temperatures in the Sylhet Division of Bangladesh. *4th Int. Conf. on Environmental Aspects of Bangladesh*, Fukoka, Japan, BENJapan, 4.

Prins, J., 2012: Process or product monitoring and control. *Engineering Statistics Handbook, NIST/SEMATECH e-Handbook of Statistical Methods*, https://www.itl.nist.gov/div898/handbook/pmc/pmc.htm.

Rajib, M. A., S. Sultana, M. Saha, and M. M. Rahman, 2014: A multi-model ensembling approach for developing plausible country-scale climate change scenarios for future. *J. Earth Sci. Climate Change*, **5**, 179, https://doi.org/10.4172/2157-7617.1000179.

Ramly, S., and W. Tahir, 2016: Application of HEC-GeoHMS and HEC-HMS as rainfall–runoff model for flood simulation. *ISFRAM 2015*, W. Tahir et al., Eds., Springer, 181–192, https://doi.org/10.1007/978-981-10-0500-8_15.

Renard, B., D. Kavetski, G. Kuczera, M. Thyer, and S. W. Franks, 2010: Understanding predictive uncertainty in hydrologic modeling: The challenge of identifying input and structural errors. *Water Resour. Res.*, **46**, W05521, https://doi.org/10.1029/2009WR008328.

Rizzo, J., 2015: A shrinking lake and a rising insurgency: Migratory responses to environmental degradation and violence in the Lake Chad basin. *The State of Environmental Migration 2015*, F. Gemenne, C. Zickgraf, and D. Lonesco, Eds., International Organization for Migration, 13–29.

Roudier, P., A. Ducharne, and L. Feyen, 2014: Climate change impacts on runoff in West Africa: A review. *Hydrol. Earth Syst. Sci.*, **18**, 2789–2801, https://doi.org/10.5194/hess-18-2789-2014.

Sarr, B., 2012: Present and future climate change in the semi-arid region of West Africa: A crucial input for practical adaptation in agriculture. *Atmos. Sci. Lett.*, **13**, 108–112, https://doi.org/10.1002/asl.368.

Schaefli, B., 2015: Projecting hydropower production under future climates: a guide for decision-makers and modelers to interpret and design climate change impact assessments. *Wiley Interdiscip. Rev.: Water*, **2**, 271–289, https://doi.org/10.1002/wat2.1083.

Serdeczny, O., and Coauthors, 2017: Climate change impacts in Sub-Saharan Africa: From physical changes to their social repercussions. *Reg. Environ. Change*, **17**, 1585–1600, https://doi.org/10.1007/s10113-015-0910-2.

Smiatek, G., H. Kunstmann, R. Knoche, and A. Marx, 2009: Precipitation and temperature statistics in high-resolution regional climate models: Evaluation for the European Alps. *J. Geophys. Res.*, **114**, D19107, https://doi.org/10.1029/2008JD011353.

Soltani, S., R. Modarres, and S. S. Eslamian, 2007: The use of time series modeling for the determination of rainfall climates of Iran. *Int. J. Climatol.*, **27**, 819–829, https://doi.org/10.1002/joc.1427.

Stanzel, P., H. Kling, and H. Bauer, 2018: Climate change impact on West African rivers under an ensemble of CORDEX climate projections. *Climate Serv.*, https://doi.org/10.1016/j.cliser.2018.05.003.

Sultan, B., and Coauthors, 2014: Robust features of future climate change impacts on sorghum yields in West Africa. *Environ. Res. Lett.*, **9**, 104006, https://doi.org/10.1088/1748-9326/9/10/104006.

Sunday, R. K. M., I. Masih, M. Werner, and P. van der Zaag, 2014: Streamflow forecasting for operational water management in the Incomati River Basin, Southern Africa. *Phys. Chem. Earth Parts ABC*, **72–75**, 1–12, https://doi.org/10.1016/j.pce.2014.09.002.

Sylla, M. B., A. T. Gaye, G. S. Jenkins, J. S. Pal, and F. Giorgi, 2010: Consistency of projected drought over the Sahel with changes in the monsoon circulation and extremes in a regional climate model projections. *J. Geophys. Res.*, **115**, D16108, https://doi.org/10.1029/2009JD012983.

——, M. Nikiema, P. Gibba, I. Kebe, and N. A. B. Klutse, 2016: Climate change over West Africa: Recent trends and future projections. *Adaptation to Climate Change and Variability in Rural West Africa*, J. Yaro and J. Hesselberg, Eds., Springer, 25–40, https://doi.org/10.1007/978-3-319-31499-0_3.

Taylor, K. E., R. J. Stouffer, and G. A. Meehl, 2012: An overview of CMIP5 and the experiment design. *Bull. Amer. Meteor. Soc.*, **93**, 485–498, https://doi.org/10.1175/BAMS-D-11-00094.1.

Tebaldi, C., and R. Knutti, 2007: The use of the multi-model ensemble in probabilistic climate projections. *Philos. Trans. Roy. Soc. London*, **365A**, 2053–2075, https://doi.org/10.1098/rsta.2007.2076.

Reyna, T., N. Guillèn, M. Laìbaque, J. Alvarez, M. Eder, and F. Funes, 2015: Using time series analysis to support the water resources management in the upper basin of the Suquía River. *Pinnacle Environ. Earth Sci.*, **2** (1), 531–539.

UNEP, 2006: *Africa's Lakes: Atlas of Our Changing Environment*. United Nations, 89 pp.

Van Liew, M. W., and J. Garbrecht, 2003: Hydrologic simulation of the little Washita River Experimental watershed using SWAT1. *J. Amer. Water Resour. Assoc.*, **39**, 413–426, https://doi.org/10.1111/j.1752-1688.2003.tb04395.x.

van Vuuren, D. P., and Coauthors, 2011: The representative concentration pathways: An overview. *Climatic Change*, **109**, 5, https://doi.org/10.1007/s10584-011-0148-z.

Verma, A., M. Jha, and R. Mahana, 2010: Evaluation of HEC-HMS and WEPP for simulating watershed runoff using remote sensing and geographical information system. *Paddy Water Environ.*, **8**, 131–144, https://doi.org/10.1007/s10333-009-0192-8.

Vizy, E. K., K. H. Cook, J. Crétat, and N. Neupane, 2013: Projections of a wetter Sahel in the twenty-first century from global and regional models. *J. Climate*, **26**, 4664–4687, https://doi.org/10.1175/JCLI-D-12-00533.1.

Wang, J., H. Ishidaira, and Z. X. Xu, 2012: Effects of climate change and human activities on inflow into the Hoabinh Reservoir in the Red River basin. *Procedia Environ. Sci.*, **13**, 1688–1698, https://doi.org/10.1016/j.proenv.2012.01.162.

Scharffenberg, W. A., and M. J. Fleming, 2010: Hydrologic modeling system HEC-HMS. User's manual, version 3.5, USACE, 318 pp., https://www.hec.usace.army.mil/software/hec-hms/documentation/HEC-HMS_Users_Manual_3.5.pdf.

Yang, L., and W. Lu, 2011: The application of time series analysis in precipitation forecast in Wuyuan County. *2011 Int. Symp. on Water Resource and Environmental Protection*, Xi'an, China, IEEE, 3063–3065, https://doi.org/10.1109/ISWREP.2011.5893525.

Yimer, G., A. Jonoski, and A. V. Griensven, 2009: Hydrological response of a catchment to climate change in the Upper Beles River basin, Upper Blue Nile, Ethiopia. Nile Basin Water Engineering Scientific Magazine, Vol. 2, 49–59.

Zema, D. A., A. Labate, D. Martino, and S. M. Zimbone, 2017: Comparing different infiltration methods of the HEC-HMS model: The case study of the Mésima Torrent (Southern Italy). *Land Degrad. Dev.*, **28**, 294–308, https://doi.org/10.1002/ldr.2591.

Zhang, J. L., Y. P. Li, G. H. Huang, C. X. Wang, and G. H. Cheng, 2016: Evaluation of uncertainties in input data and parameters of a hydrological model using a Bayesian Framework: A case study of a snowmelt–precipitation-driven watershed. *J. Hydrometeor.*, **17**, 2333–2350, https://doi.org/10.1175/JHM-D-15-0236.1.

Zhu, H., Y. Li, Y. Huang, Y. Li, C. Hou, and X. Shi, 2018: Evaluation and hydrological application of satellite-based precipitation datasets in driving hydrological models over the Huifa river basin in Northeast China. *Atmos. Res.*, **207**, 28–41, https://doi.org/10.1016/j.atmosres.2018.02.022.

Zubler, E. M., M. Fischer Andreas, F. Fröb, and A. Liniger Mark, 2016: Climate change signals of CMIP5 general circulation models over the Alps – Impact of model selection. *Int. J. Climatol.*, **36**, 3088–3104, https://doi.org/10.1002/joc.4538.